Available online at www.sciencedirect.com
ScienceDirect
Geochimica et Cosmochimica Acta 71 (2007) 5635–5650
Geochimica et Cosmochimica Acta
www.elsevier.com/locate/gca

Dissolution mechanisms of goethite in the presence of siderophores and organic acids

P.U. Reichard [a], R. Kretzschmar [a], S.M. Kraemer [b,*]

[a] Institute of Biogeochemistry and Pollutant Dynamics, ETH Zurich, CHN, 8092 Zurich, Switzerland
[b] Department of Environmental Geosciences, University of Vienna, Althanstrasse 14, 1090 Vienna, Austria

Received 8 May 2006; accepted in revised form 27 December 2006; available online 20 February 2007

Abstract

In dynamic natural systems such as soils and surface waters, transient biogeochemical processes can induce strong chemical non-steady-state conditions. In this paper, we investigate the effects of non-steady-state conditions on ligand-controlled iron oxide dissolution. The rates of goethite dissolution at pH 6 in the presence of low molecular weight organic acids (oxalate, citrate or malonate) were observed. Non-steady-state conditions were induced by rapid additions of fungal, bacterial or plant siderophores. In the presence of the low molecular weight organic acids, dissolved iron concentrations are below detection limit as predicted by equilibrium solubility calculations. The rapid addition of the siderophores triggered reproducible, fast dissolution of kinetically labile iron from the iron oxide surface. The same effect was observed upon rapid additions of high citrate concentrations to goethite-oxalate suspensions. The concentration of the labile iron pool at the mineral surface was a function of the surface concentration of the low molecular weight organic acids and of the reaction time before addition of the siderophores. Isotopic exchange with ^{59}Fe independently confirmed the existence of the labile iron pool before addition of the siderophore. A dissolution mechanism was elucidated that is consistent with these observations and with accepted models of ligand-controlled dissolution. We conclude that the fast dissolution reaction observed here is an important process in biological iron acquisition and that it is based on a general geochemical mechanism.

1. INTRODUCTION

Iron is an essential micronutrient for most known organisms. However, the low solubility of iron oxides near neutral pH contributes to the low availability of iron to plants and microorganisms in natural systems such as calcareous soils and marine water. In calcareous soils, the pore water pH is controlled by the solubility of calcite and the CO_2 partial pressure in the gas phase. In the presence of high CO_2 partial pressures typically observed in the rhizosphere (Gollany et al., 1993) the equilibrium pH of soil solutions is between pH 6 and 7. Under these conditions, organisms increase the bioavailability of iron using specific iron acquisition strategies. An efficient biological iron acquisition strategy of bacteria, fungi, and graminaceous plants involves the production and exudation of siderophores (Neilands, 1974; Römheld and Marschner, 1986; Watteau and Berthelin, 1994; Telford and Raymond, 1996; Albrecht-Gary and Crumbliss, 1998). Siderophores are defined as iron specific organic ligands of biological origin that are released by organisms under iron-deficiency (please note that we use the term 'siderophore' only for compounds that conform to this definition, and that we use the term 'ligand' for all other organic ligands). Siderophores promote the dissolution of iron-bearing minerals including iron oxides (e.g. Watteau and Berthelin, 1994; Hersman et al., 1995; Holmen and Casey, 1996; Kraemer et al., 1999; Kalinowski et al., 2000; Cervini-Silva and Sposito, 2002; Kraemer, 2004; Borer et al., 2005).

To understand the mechanisms of iron acquisition in soils, two important factors need to be taken into account: the chemical complexity and the dynamics of soil systems.

* Corresponding author. Fax: +43 1 4277 9543.
E-mail address: stephan.kraemer@univie.ac.at (S.M. Kraemer).

0016-7037/$ - see front matter © 2007 Elsevier Ltd. All rights reserved.
doi:10.1016/j.gca.2006.12.022

Chemical complexity in the rhizosphere includes the presence of organic ligands which may interfere with biological iron acquisition. For example, low molecular weight organic acids such as oxalate are virtually ubiquitous in soils (Gadd, 2000). The concentration of oxalic acid in natural systems ranges from 2.5×10^{-5} to 4.0×10^{-3} M (Fox and Comerford, 1990; Allison et al., 1995; Vance et al., 1996). Also, a full characterization of root exudation by iron stressed barley plants has shown that a range of organic acids including fumarate, lactate, malate as well as various amino acids are co-exuded with siderophores under iron limiting conditions (Fan et al., 1997). Similarly, root exudation of malic acid by wheat plants has been observed (Dakora and Phillips, 2002). Watteau and Berthelin (1994) found that the siderophore-exuding fungus *Suillus granulatus* initially exuded aliphatic acids under iron deficiency, and only later released siderophores. The importance of organic ligands other than siderophores in biological iron acquisition was demonstrated by the observation of a strong synergistic effect of oxalate on siderophore-controlled dissolution of iron oxides (Cheah et al., 2003). The effect of siderophores and organic acids on the solubility of goethite is shown in Figure EA-1 of the electronic annex.

Non-stationary conditions are commonly observed in natural systems. The dynamics of natural systems are introduced by many processes including microbial and root growth or decay, diurnal variations in the release of exudates, and uptake of water and nutrients. The diurnal regulation of biological iron acquisition by iron deficient graminaceous plants (e.g. barley and wheat) is an example of such a process. The release of siderophores by the plant roots starts shortly after sunrise, continues for about 4 h, and declines thereafter (Takagi et al., 1984; Römheld and Marschner, 1986). Despite the reduced iron acquisition during the rest of the day, this pulse release of phytosiderophores is sufficient to mobilize enough iron to meet the daily demand of the plants (Römheld, 1991; Takagi, 1993). It has been estimated that transient siderophore concentrations in the rhizosphere during the maximum exudation period are in the millimolar range close to the root surface (Römheld, 1991). This exudation pattern introduces distinct changes in the solubility. Moreover, several studies have shown that rapid changes in the geochemical environment including rapid changes in pH, solution saturation state, and ligand concentrations can trigger fast mineral dissolution reactions (Mast and Drever, 1987; Samson and Eggleston, 1998; Samson and Eggleston, 2000; Teng et al., 2001; Pokrovsky and Schott, 2004).

The effect of siderophores and other organic ligands on iron oxide dissolution has been described as a ligand-controlled dissolution mechanism (Furrer and Stumm, 1986; Kraemer et al., 1999). Therefore, we apply the term 'ligand-controlled dissolution' to dissolution mechanisms involving siderophores as well as other organic or inorganic ligands in the subsequent discussion.

Ligand-controlled dissolution is a surface controlled process to which an empirical rate law can be applied where the net dissolution rate is a function of the surface concentration of the adsorbed ligands (Furrer and Stumm, 1986) and of the solution saturation state (Kraemer and Hering, 1997):

$$R_L = k_{L_i}[L_i]^n_{ads} f(\Delta G) \quad (1)$$

where R_L [nmol m^{-2} h^{-1}] is the ligand-controlled dissolution rate. R_L is the rate of a dissolution reactions promoted by the ligand L_i. k_{L_i} [h^{-1}] is the rate coefficient of dissolution promoted by the ligand L_i, $[L_i]_{ads}$ [nmol m^{-2}] is the adsorbed ligand concentration and the superscript n is a rate order. Previous studies on ligand-controlled dissolution involving multidentate ligands have found rate orders $n = 1$ (e.g. Furrer and Stumm, 1986; Casey and Ludwig, 1996; Holmen and Casey, 1996). $f(\Delta G)$ is a function of the solution saturation state with respect to the dissolving mineral expressed as Gibbs free energy of reaction (Lasaga, 1981; Aagaard and Helgeson, 1982). It is zero at equilibrium and approaches unity at strong undersaturation. For ligand-controlled dissolution $f(\Delta G)$ has the form

$$f(\Delta G) = \left[1 - \exp\left(\frac{\Delta G}{\sigma RT}\right)\right] \quad (2)$$

where ΔG [kJ $mole^{-1}$] is the Gibbs free energy of reaction, R is the molar gas constant [J K^{-1} mol^{-1}] and T is the absolute temperature [K], σ is the Temkins coefficient (Temkin, 1971) which was empirically determined as two for ligand controlled dissolution of goethite in the presence of the ligand 8-hydroxyquinoline-5-sulfonate (Kraemer and Hering, 1997).

A central assumption made in the interpretation of ligand-controlled dissolution is that parallel dissolution mechanisms (including proton-promoted and all ligand-promoted mechanisms) are independent:

$$R = R_H + \sum R_{L_i} \quad (3)$$

where R, R_H, and $\sum R_{L_i}$ [mol m^{-2} h^{-1}] are the overall dissolution rate, the proton-promoted dissolution rate, and the sum of the rates of all parallel dissolution reactions promoted by the ligands L_i. In most instances, this model of independent dissolution mechanisms has been consistent with observations (e.g. Bondietti et al., 1993; Cervini-Silva and Sposito, 2002; Cheah et al., 2003). However, Kraemer et al. (1998) reported that mechanisms of ligand-controlled aluminum oxide dissolution in the presence of a bidentate organic ligand (8-hydroxyquinolinole-5-sulfonate) and small inorganic ligands such as fluoride were not independent.

The independence of proton-promoted and ligand-promoted processes can be difficult to ascertain as changes in pH can affect both the rates of proton-promoted and ligand-promoted dissolution. For example, changes in pH can influence ligand-controlled dissolution by modifying the concentrations and speciation of adsorbed ligands. pH dependent protonation of the adsorbed ligand can result in an apparent shift in the rate coefficient k_{Li}, (Nowack and Sigg, 1997) unless the rate law contains separate terms for each surface species of the ligand L_i with corresponding (pH-independent) rate coefficients. However, some studies found that the rate coefficient of ligand-controlled dissolution depended on the overall surface protonation state even though the protonation state of the adsorbed ligand was assumed to be constant (Zinder et al., 1986; Holmen and Casey, 1996). Casey and Ludwig (1996) suggested that this dependency arises from the protonation of disrupted bonds

between the detaching metal center and bridging oxygen of the crystal lattice. In the study presented here, the pH has been kept constant, so that we assume that the surface speciation of the ligands as well as the surface protonation state remain constant.

Cheah et al. (2003) applied the rate laws Eqs. (1) and (3) to ligand-controlled goethite dissolution in the presence of the microbial siderophore desferrioxamine-B (DFO-B) and oxalate (Ox) at pH 5 and far from equilibrium (i.e. $f(\Delta G) = 1$):

$$R = R_H + k_{DFO}[DFO - B]_{ads} + k_{Ox}[Ox]_{ads} \quad (4)$$

Proton-promoted dissolution rates at pH 5 were found to be negligible compared to ligand-controlled dissolution rates (Cheah et al., 2003) so that the rate law simplified to:

$$R = k_{DFO}[DFO - B]_{ads} + k_{Ox}[Ox]_{ads} \quad (5)$$

As indicated by Eq. (5), oxalate and DFO-B promote dissolution by a surface-controlled mechanism if the solution is under-saturated with respect to goethite. However, Cheah et al. (2003) also observed that DFO-B influences dissolution by its strong effect on the solution saturation state (even at small free dissolved DFO-B concentrations) due to its high affinity for iron complexation as predicted by thermodynamic calculations. In the absence of the siderophore, oxalate-promoted dissolution was limited by the low solubility of goethite at pH 5. Consequently, in the presence of less than 1.0×10^{-4} M dissolved oxalate, equilibrium was reached at very low dissolved iron concentrations and net dissolution rates approached zero. In the simultaneous presence of the siderophore and oxalate, the system was strongly under-saturated with respect to goethite and both surface-controlled processes (siderophore-controlled dissolution and oxalate-controlled dissolution) were occurring at maximum rates. In summary, the effect of the siderophore on ligand-controlled dissolution was twofold: it adsorbed to the surface and served as a reactant in a ligand-controlled dissolution mechanism; and it complexed dissolved iron and shifted the solution saturation state retaining far from equilibrium conditions. This led to an apparent synergistic effect where the sum of the net dissolution rates observed in single ligand systems (siderophore or oxalate) was lower than the net dissolution rates in the presence of both ligands. Eq. (5) does not account for the effect of DFO-B on dissolution rates by modification of the solution saturation state.

In this study, we further investigate goethite dissolution in the presence of various organic ligands and DFO-B. Moreover, we investigate the effect of rapid siderophore additions on goethite dissolution in the presence and in the absence of other ligands. While previous studies have focused on iron oxide dissolution in the presence of constant siderophore concentrations, these 'non-steady-state experiments' are intended to mimic rapid changes in soil chemical environments as a consequence of pulse releases of plant siderophores into the rhizosphere as discussed above. Based on observations presented here, we propose a conceptual model which describes ligand-controlled dissolution at constant total ligand concentrations as well as non-steady-state dissolution.

2. MATERIALS AND METHODS

2.1. Materials

Goethite was synthesized following a method of Schwertmann and Cornell (2000). Briefly, 180 mL of 5 M KOH (ACS grade; Fluka) solution were added rapidly to 100 mL of 1 M $Fe(NO_3)_3$ (ACS grade; Sigma) solution while stirring vigorously. High-purity water (18 MΩ, Milli-Q, Millipore) was added to the suspension to reach a final volume of 2 L. The suspension was heated at 70 °C for 60 h. The product was repeatedly washed and centrifuged with high-purity water until the pH of the supernatant was near neutral. After the final washing, the product was centrifuged and freeze dried. X-ray powder diffraction confirmed the goethite structure of the synthesized mineral. The specific surface area was determined as 38 $m^2\ g^{-1}$ by a multipoint N_2-BET adsorption method (surface area analyzer Gemini 2360, Micromeritics).

The siderophores DFO-B (desferrioxamine-B mesylate; Ciba-Geigy) and ferrichrome (Sigma) were used as received. Phytosiderophores were obtained by growing wheat (*Triticum aestivum* L. cv. Tamaro) hydroponically in an iron free nutrient solution (Reichard, 2005) according to Neumann et al. (1999). Initial growth of the plant in iron free nutrient solution is sustained by iron in the seed (Marschner, 1995). The plant roots exuded the phytosiderophore DMA (2′-deoxymugineic acid) which was purified following an adapted method of Neumann et al. (1999). The procedure involves sequential purification by cation exchange chromatography (Dowex 50 WX2; Serva), size exclusion chromatography (Sephadex G-10; Amersham–Pharmacia) and metal exchange chromatography (Chelex 100; Bio-Rad) (Reichard, 2005).

Oxalate (di-sodium oxalate; Merck), citrate (tri-sodium citrate dihydrate; Merck), succinate (butanedioic acid; Sigma–Aldrich), fumarate (fumaric acid; Sigma–Aldrich) and malonate (propanedioic acid; Sigma) and all other chemicals were analytical grade. All solutions were prepared with high-purity water (18 MΩ, Milli-Q, Millipore). 0.013 mL of a ^{59}Fe-labeled solution with an activity of 298 MBq mL^{-1} and a total iron concentration of 0.0056 M (manufacturer specifications) was purchased (Amersham Bioscience). A stock solution was prepared by acidification with concentrated $HClO_4$ (Fluka) and dilution of the total solution volume (i.e. 0.013 mL) to 1 mL. The solid ^{14}C-labeled oxalate (Sigma) was dissolved in 10 mL high-purity water resulting in an activity of 93 KBq mL^{-1}.

All dissolution experiments and the oxalate adsorption isotherm experiment were performed in 0.01 M $NaClO_4$ (sodium perchlorate monohydrate, Merck) buffered to pH 6 with 0.005 M Mops (3-morpholinepropanesulfonic acid; Fluka). This buffer has no influence on goethite dissolution (Kraemer et al., 1999). The pH values of the solutions and suspensions were adjusted with perchloric acid or sodium hydroxide solutions. Samples were filtered using plastic syringe filter holders (Schleicher andSchuell) with 0.025 μm cellulose nitrate membranes (Schleicher and Schuell).

Total dissolved iron concentrations were measured with ICP-MS (Agilent 7500a) (detection limit: 2.0×10^{-7} M Fe).

Standards were prepared by dilution of an iron atomic spectroscopy standard solution (Fluka) and acidification with HNO_3 (Suprapur; Merck). Prior to analysis, samples were stabilized by acidification with HNO_3 (Suprapur; Merck).

2.2. Adsorption experiments

All adsorption experiments were conducted in batch reactors with a volume of 2.5 mL and goethite solid concentrations of 2.5 g L^{-1}. The reactors were open to the atmosphere at ambient temperature (23 ± 3 °C). The solids were continuously suspended by a magnetic stirrer. Adsorption of oxalate on goethite was measured at pH 6. Two replicates of goethite–oxalate suspensions and one series of blanks were prepared. Blanks were prepared analogously, but without goethite. The same concentration of ^{14}C-labeled oxalate (1.5×10^{-5} M) was added to each batch, except for the oxalate-free samples. Total oxalate concentrations were 2.5×10^{-5}, 5.0×10^{-5}, 7.5×10^{-5}, 1.0×10^{-4}, 1.5×10^{-4}, 2.5×10^{-4} and 5.0×10^{-4} M. After a reaction time of 0.5 h, the samples were filtered. The first mL of the filtrate was discarded and 0.5 mL was collected for the measurement of the activity of ^{14}C with a scintillation counter Liquid Scintillation Analyzer 2200CA; Packard.

Competitive adsorption between oxalate and DFO-B was determined at total concentrations of 4.0×10^{-5} M DFO-B and 1.0×10^{-4} M oxalate (i.e. 1.5×10^{-5} M ^{14}C-labeled oxalate and 8.5×10^{-5} M non-labeled oxalate). The ligands were added simultaneously. Two replicates were prepared. After a reaction time of 0.5 h, the samples were filtered.

Adsorption of DFO-B on goethite was determined at a total concentration of 5.0×10^{-5} M DFO-B. The dissolved DFO-B concentration was measured with a Cary 1E UV–Visible spectrophotometer at 439 nm as Fe–DFO-B complex in the presence of excess Fe at pH 1.5 (Kraemer et al., 1999). Dissolved iron concentrations in adsorption experiments were always below 1.0×10^{-6} M (ICP-MS).

2.3. Dissolution experiments

All dissolution experiments were conducted in 300 mL high density polyethylene (HDPE) batch reactors containing goethite suspensions with solid concentrations of 2.5 g L^{-1} at an ionic strength of 0.01 M ($NaClO_4$) and at pH $= 6.0 \pm 0.05$. The reactors were wrapped with aluminum foil to exclude light and shaken continuously on an end-over-end shaker at ambient temperature. Samples were taken over time and filtered. The first 2 mL of the filtrate were discarded and 5 mL were collected and immediately frozen.

Two types of dissolution experiments were conducted: batch dissolution experiments at constant total ligand concentrations and non-steady-state experiments. Goethite dissolution in the presence of constant total ligand concentration of 5.0×10^{-5} M DFO-B was compared to dissolution in the presence of 5.0×10^{-5} M DFO-B and 5.0×10^{-5} M of an additional organic ligand (i.e. oxalate, citrate, malonate, succinate or fumarate, respectively).

Non-steady-state experiments were conducted in the presence of low molecular weight organic acids including 5.0×10^{-5} or 1.0×10^{-4} M oxalate, 5.0×10^{-4} M citrate, or 7.5×10^{-4} M malonate. Non-steady-state conditions were induced by addition of 3.8×10^{-6}, 6.0×10^{-6}, 6.4×10^{-6}, or 4.0×10^{-5} M DFO-B, 4.0×10^{-5} M ferrichrome, 3.0×10^{-3} M DMA, or 3.0×10^{-3} M citrate to the suspensions. These ligands were added at variable times after the start of the dissolution experiment.

To investigate the effect of increasing oxalate concentrations on non-steady-state dissolution, 0, 2.5×10^{-5}, 5.0×10^{-5}, 7.5×10^{-5} or 1.0×10^{-4} M oxalate was added to goethite suspensions at $t = 0$ h. After 210 h, each suspension was spiked with 4.0×10^{-5} M DFO-B to induce non-steady-state conditions.

2.4. Isotopic exchange

For the isotopic exchange experiment, a goethite suspension (solid concentration: 2.5 g L^{-1}, $I = 0.01$ M ($NaClO_4$), pH $= 6.0 \pm 0.05$) containing 8.0×10^{-3} M oxalate was prepared. The sample container was wrapped with aluminum foil to exclude light and the suspension was left on an end-over-end shaker for 1490 h. Then, 100 mL suspension was spiked with 10 μL of the stock solution containing ^{59}Fe-labeled iron resulting in a total iron addition of 7.28×10^{-9} M and a measured activity of 328 Bq mL^{-1}. A control experiment containing no goethite was prepared analogously to the iron suspension and spiked with ^{59}Fe-labeled iron so that it had the same activity at the beginning of the experiment. Immediately, after adding the radioactive tracer and periodically thereafter, samples of the blank and the suspension were taken and filtered. Total dissolved iron concentrations in the filtrate were measured by ICP-MS and the activity of the dissolved ^{59}Fe was measured with a scintillation counter (Liquid Scintillation Analyzer 2200CA; Packard). A decrease of activities due to natural decay of ^{59}Fe ($t_{1/2} = 44.51$ day (Unterweger et al., 2001)) was taken into account by reporting the ratios of the activity of the filtered suspension versus the activity of the (filtered) control sample.Twenty nine hour after the addition of ^{59}Fe-labeled iron ($t = 1519$ h), 1.0×10^{-4} M DFO-B were added to induce non-steady-state conditions. Sampling of the control solution and of the suspension was continued after the DFO-B addition for approximately 20 h.

3. RESULTS AND DISCUSSION

3.1. Adsorption studies

Fig. 1 shows the adsorption of oxalate onto goethite at pH 6. The adsorption data were fitted with the Freundlich isotherm model $[Ox_{ads}] = K_d \times [Ox]^{\frac{1}{n}}$ with a $K_d = 1.0661 \times 10^{-5}$ L m^{-2} and $\frac{1}{n} = 0.3096$ where $[Ox_{ads}]$ and [Ox] are the adsorbed and soluble oxalate concentrations, respectively. An adsorbed oxalate concentration of 5.35×10^{-7} mol m^{-2} was observed at a total oxalate concentration of 1.0×10^{-4} M at pH 6. At the same pH

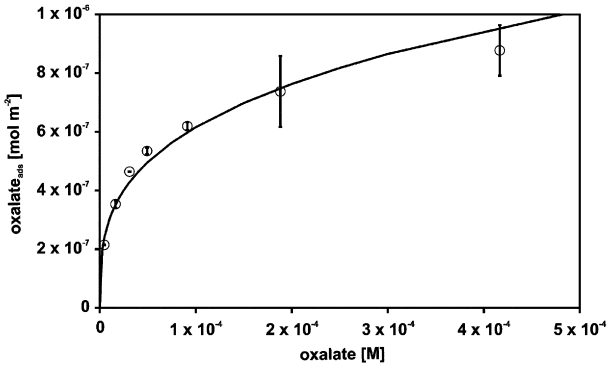

Fig. 1. Adsorption isotherm for oxalate adsorption onto goethite. Total oxalate concentrations: 2.5×10^{-5}, 5.0×10^{-5}, 7.5×10^{-5}, 1.0×10^{-4}, 1.5×10^{-4}, 2.5×10^{-4} and 5.0×10^{-4} M. Solid concentration of goethite 2.5 g L^{-1}, ionic strength: 0.01 M ($NaClO_4$), 0.005 M buffer (Mops), pH 6. The solid line represents a Freundlich isotherm model with $K_d = 1.0661\times10^{-5}$ L m^{-2} and $\frac{1}{n} = 0.3096$.

an adsorbed DFO-B concentration of 6.1×10^{-8} mol m^{-2} was measured in the presence of 5.0×10^{-5} M DFO-B. In a binary system containing total oxalate and DFO-B concentrations of 1.0×10^{-4} M and 4.0×10^{-5} M, respectively, adsorbed concentrations of 5.25×10^{-7} mol m^{-2} oxalate and 2.9×10^{-8} mol m^{-2} DFO-B were observed, indicating a minor effect of adsorption competition between DFO-B and oxalate .

3.2. Dissolution of goethite at constant total ligand concentrations

Fig. 2 shows dissolved iron concentrations as a function of time in goethite dissolution experiments containing 5.0×10^{-5} M DFO-B alone or 5.0×10^{-5} M DFO-B and 5.0×10^{-5} M of other organic ligands including oxalate, fumarate, malonate, succinate, and citrate, respectively. After a somewhat faster initial increase of iron concentrations as a function of time, the net dissolution rates remain approximately constant after 60 h. Fast initial dissolution is commonly observed in iron oxide dissolution studies (see e.g. Zinder et al., 1986). The slopes (with 95% confidence limits) of linear least-squares fits of the data (with $t \geqslant 60$ h) are reported as net dissolution rates as listed in Table 3.

The net dissolution rate in the presence of 5.0×10^{-5} M DFO-B only is $2.9\times10^{-10}\pm0.4\times10^{-10}$ mol m^{-2} h^{-1}. Assuming that the proton-promoted dissolution rate is essentially zero at pH 6 (Cheah et al., 2003), a rate coefficient for goethite dissolution in the presence of DFO-B can be calculated based on the rate law Eq. (6) using the rate order of unity for DFO-B promoted dissolution (Cheah et al., 2003):

$$R_{DFO} = k_{DFO}[DFO-B]_{ads} \quad (6)$$

In the presence of a total concentration of 5.0×10^{-5} M DFO-B at pH 6 we observed an adsorbed DFO-B concentration $[DFO\text{-}B]_{ads} = 6.1\times10^{-8}$ mol m^{-2} so that the dissolution rate coefficient according to Eq. (6) is $k_{DFO} = 0.0048$ h^{-1}. The net dissolution rates do not decrease at high dissolved iron concentrations despite the formation of Fe–DFO-B complexes and a concomitant decrease of the free DFO-B concentrations which could in turn lead to a decrease of adsorbed DFO-B. However, previous observations of DFO-B adsorption on goethite showed constant maximum DFO-B surface concentrations at free dissolved DFO-B concentrations at or above 2.5×10^{-5} M (Kraemer et al., 1999). Therefore, we do not expect a significant change in the adsorbed DFO-B concentration under the experimental conditions. Due to the extremely high affinity of DFO-B for iron, the solubility of goethite in the presence of the siderophore is controlled by the soluble siderophore concentration. Calculated ΔG values remain below -12 kJ/mole^{-1} as long as only 0.4% of free siderophore remains in solution. Therefore, we would expect according to Eq. (2) that the reaction rate remains above 90% of the maximum rate as long as the soluble iron concentration is less then 4.98×10^{-5} M at a soluble DFO-B concentration of 5.0×10^{-5} M.

Slightly higher goethite net dissolution rates were observed in the presence of 5.0×10^{-5} M DFO-B and 5.0×10^{-5} M of fumarate, malonate or succinate, ($R_{DFO,fumarate} = 5.1\times10^{-10}\pm0.3\times10^{-10}$ mol m^{-2} h^{-1}; $R_{DFO,malonate} = 4.4\times10^{-10}\pm0.7\times10^{-10}$ mol m^{-2} h^{-1}; $R_{DFO,succinate} = 3.7\times10^{-10}\pm0.3\times10^{-10}$ mol m^{-2} h^{-1}). Citrate had an inhibitory effect on the DFO-B-controlled dissolution ($R_{DFO,citrate} = 1.7\times10^{-10}\pm0.5\times10^{-10}$ mol m^{-2} h^{-1}). The highest net dissolution rates were observed in the presence of oxalate and DFO-B. In this case, the net dissolution rate was almost 2.5 times higher ($R_{DFO,oxalate} = 6.7\times10^{-10}\pm1.0\times10^{-10}$ mol m^{-2} h^{-1}) than the net rates in the presence of DFO-B alone. Using the model for ligand-controlled dissolution in the presence of two ligands as proposed by Cheah et al. (2003) (Eq. 5), the dissolution rate coefficient k_{ox} (oxalate-promoted dissolution) was calculated based on adsorption and dissolution experiments conducted at total dissolved concentrations of 4.0×10^{-5} M DFO-B and 1.0×10^{-4} M oxalate at pH 6. Under these conditions, $[oxalate]_{ads} = 5.25\times10^{-7}$ mol m^{-2}, $[DFO\text{-}B]_{ads} = 2.9\times10^{-7}$ mol m^{-2}, and $R_{DFO,oxalate} = 8.1\times10^{-10}\pm1.4\times10^{-10}$ mol m^{-2} h^{-1} (Table 3, rate determined from dissolution experiment shown in Fig. 6a). As discussed above, k_{DFO} at this pH is 0.0048 h^{-1}. Based on these parameters, Eq. (5) was solved for the dissolution rate coefficient $k_{ox} = 0.0013$ h^{-1}.

The data for the DFO-B-promoted and the oxalate–DFO-B-promoted dissolution are in good agreement with the data from Cheah et al. (2003). They calculated a somewhat higher rate coefficient for goethite dissolution in the presence of DFO-B ($k_{DFO} = 0.015$ h^{-1}) at pH 5. Their calculated rate coefficient of oxalate-promoted dissolution at pH 5 ($k_{ox} = 0.001$ h^{-1}) is in good agreement with our observations.

The low molecular weight organic acids selected in this study represent common organic compounds in a range of natural systems including soils and surface waters (Stevenson, 1967; Fan et al., 1997; Gadd, 2000; Strobel, 2001). In the simultaneous presence of the siderophore and one of these organic acids, the dissolution reaction was not limited by a solubility equilibrium under the experimental conditions. This led to a synergistic effect on net dissolution rates in the presence of DFO-B and oxalate that

Table 1
Thermodynamic equilibrium constants at 298.15 K for the low molecular weight organic acids oxalate, fumarate, malonate, succinate, and citrate and for the siderophores DFO-B, ferrichrome, and DMA

Reaction	log K_{298}
Oxalate	
$C_2O_4^{2-} + H^+ = HC_2O_4^-$	4.27[a]
$C_2O_4^{2-} + 2H^+ = H_2C_2O_4$	1.25[a]
$C_2O_4^{2-} + Fe^{3+} = FeC_2O_4^+$	8.804[a]
$2C_2O_4^{2-} + Fe^{3+} = Fe(C_2O_4)_2^-$	15.136[a]
$3C_2O_4^{2-} + Fe^{3+} = Fe(C_2O_4)_3^{3-}$	19.824[a]
Fumarate	
$H_2C_4O_4^{2-} + H^+ = H_3C_4O_4^-$	4.48[a]
$H_3C_4O_4^- + H^+ = H_4C_4O_4$	3.02[a]
Malonate	
$H_2C_3O_4^{2-} + H^+ = H_3C_3O_4^-$	5.696[a]
$H_3C_3O_4^- + H^+ = H_4C_3O_4$	2.847[a]
$H_2C_3O_4^{2-} + Fe^{3+} = FeH_2C_3O_4^+$	9.401[a]
$2H_2C_3O_4^{2-} + Fe^{3+} = Fe(H_2C_3O_4)_2^-$	15.708[a]
$3H_2C_3O_4^{2-} + Fe^{3+} = Fe(H_2C_3O_4)_3^{3-}$	18.513[a]
Succinate	
$H_4C_4O_4^{2-} + H^+ = H_5C_4O_4^-$	5.636[a]
$H_5C_4O_4^- + H^+ = H_6C_4O_4$	4.207[a]
$H_4C_4O_4^{2-} + Fe^{3+} = FeH_4C_4O_4^+$	8.466[a]
Citrate	
$H_5C_6O_7^{3-} + H^+ = H_6C_6O_7^{2-}$	6.396[a]
$H_6C_6O_7^{2-} + H^+ = H_7C_6O_7^-$	4.761[a]
$H_7C_6O_7^- + H^+ = H_8C_6O_7$	3.128[a]
$H_6C_6O_7^{3-} + Fe^{3+} = FeH_6C_6O_7$	13.004[a]
$H_7C_6O_7^{2-} + Fe^{3+} = FeH_7C_6O_7^+$	7.981[a]
$FeH_6C_6O_7 + H_2O = FeH_7C_6O_8^- + H^+$	−2.913[a]
$2H_6C_6O_7^{3-} + 2Fe^{3+} + 2OH^- = Fe_2(OH)_2(H_6C_6O_7)_2^{2-}$	24.402[a]
DFO-B	
$DFOB^{3-} + H^+ = HDFOB^{-2}$	11.43[a]
$HDFOB^{2-} + H^+ = H_2DFOB^-$	21.41[a]
$H_2DFOB^- + H^+ = H_3DFOB$	30.59[a]
$H_3DFOB + H^+ = H_4DFOB^+$	38.91[a]
$DFOB^{3-} + Fe^{3+} + H^+ = FeHDFOB^+$	43.42[a]
$DFOB^{3-} + Fe^{3+} + 2\ H^+ = FeH_2DFOB^{+2}$	44.11[a]
$FeDFOB + H^+ = HFeDFOB^+$	10.40[a]
Ferrichrome	
$Fchr^{3-} + H^+ = HFchr^{2-}$	10.47[a]
$HFchr^{2-} + H^+ = H_2Fchr^-$	9.427[a]
$H_2Fchr^- + H^+ = H_3Fchr$	8.323[a]
$Fchr^{3-} + Fe^{3+} = FeFchr$	30.991[a]
$FeFchr + H^+ = HFeFchr^+$	1.5[a]
DMA	
$H_4DMA^+ + H^+ = H_5DMA^{2+}$	2.13[b]
$H_3DMA + H^+ = H_4DMA^+$	2.74[b]
$H_2DMA^- + H^+ = H_3DMA$	3.41[c]
$HDMA^{2-} + H^+ = H_2DMA^-$	8.69[c]
$DMA^{3-} + H^+ = HDMA^{2-}$	10.66[c]
$DMA^{3-} + Fe^{3+} = FeDMA$	20.36[c]
$DMA^{3-} + Fe^{3+} + H_2O = FeOHDMA^- + H^+$	18.01[c]
Fe^{3+}	
$H_2O + Fe^{3+} = FeOH^{2+} + H^+$	−2.19[a]
$2H_2O + Fe^{3+} = Fe(OH)_2^+ + 2H^+$	−4.69[a]
Goethite	
$2\ H_2O + Fe^{3+} = FeOOH(s) + 3\ H^+$	−0.36[d]

Conditional equilibrium constants from [a] Martell et al. (2001); [b] Sugiura et al. (1981); [c] Murakami et al. (1989); [d] Parker and Khodakovskii (1995). Corrected to zero ionic strength with Davies equation.

Table 2
Calculated equilibrium concentrations of iron before DFO-B addition and dissolved iron concentration after DFO-B addition for goethite dissolution at pH 6 in the presence of oxalate, malonate, succinate, citrate or fumarate

Organic acid (5.0×10^{-5} M)	Max. $[Fe]_{diss}$, before DFO-B addition[a] [M]	Max. observed $[Fe]_{diss}$, after DFO-B addition[b] [M]	ΔG after DFO-B addition[c] [kJ mol^{-1}]
Oxalate	6.9×10^{-11}	2.77×10^{-5}	−28.6
Malonate	6.0×10^{-11}	1.43×10^{-5}	−29.2
Succinate	5.2×10^{-11}	1.10×10^{-5}	−30.9
Citrate	1.9×10^{-7}	7.70×10^{-6}	−32.1
Fumarate[d]	—	1.36×10^{-5}	—

[a] Calculated equilibrium concentrations of dissolved iron in the absence of DFO-B. The concentrations are approximately equal since the solubility of iron under these conditions is determined by hydrolysis species and not by organic complexes.
[b] Highest measured $[Fe]_{diss}$ during experiment.
[c] Calculated for the highest measured $[Fe]_{diss}$ during each experiment.
[d] Thermodynamic stability constants for Fe–fumarate complexes were not available (see Table 1).

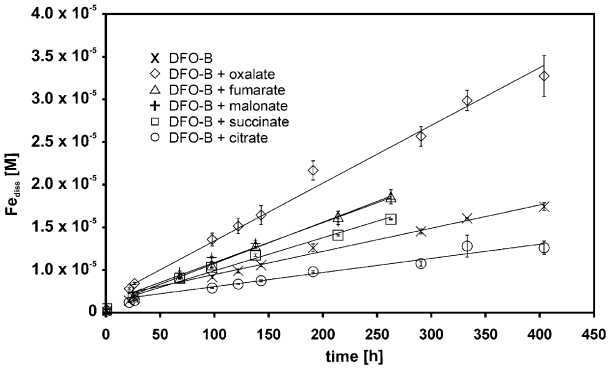

Fig. 2. Dissolution of goethite in the presence of constant total concentrations (5.0×10^{-5} M) of DFO-B (X) and of DFO-B combined with an additional organic acid (open symbols and cross) including oxalate, fumarate, malonate, succinate, and citrate. Solid conc.: 2.5 g L^{-1}, I = 0.01 M ($NaClO_4$), pH 6. Solid lines represent linear regression fit for each dissolution data. The calculated rates and 95% confidence limits for the slope of the regression lines are listed in Table 3.

Table 3
Net dissolution rates for goethite at pH 6 in the presence of different organic ligands

Organic acid	Organic acid [M]	DFO-B [M]	R_L [mol m^{-2} h^{-1}]
—	—	5×10^{-5}	$2.9\times10^{-10}\pm0.4\times10^{-10}$
Oxalate	5×10^{-5}	5×10^{-5}	$6.7\times10^{-10}\pm1.0\times10^{-10}$
Oxalate	1×10^{-4}	4×10^{-5}	$8.1\times10^{-10}\pm1.4\times10^{-10}$
Fumarate	5×10^{-5}	5×10^{-5}	$5.1\times10^{-10}\pm0.3\times10^{-10}$
Malonate	5×10^{-5}	5×10^{-5}	$4.4\times10^{-10}\pm0.7\times10^{-10}$
Succinate	5×10^{-5}	5×10^{-5}	$3.7\times10^{-10}\pm0.3\times10^{-10}$
Citrate	5×10^{-5}	5×10^{-5}	$1.7\times10^{-10}\pm0.5\times10^{-10}$

Dissolution rates were calculated by linear regression of data in Figs. 2 and 6a and normalization to the goethite surface area. The errors represent the 95% confidence limits on the slope of regression calculations.

was previously observed by Cheah et al. (2003). Similar synergistic effects were observed in the presence of DFO-B and fumarate, malonate, or succinate, respectively. The selected ligands possess carboxylic functional groups and form bidentate inner sphere complexes with the surface iron (Cornell and Schindler, 1980; Filius et al., 1997). Furrer and Stumm (1986) found that ligands such as oxalate forming five-membered chelate rings at the surface are most effective in promoting dissolution, followed by six-membered ring forming ligands, like malonate.

The presence of citrate led to an inhibition of DFO-B-controlled dissolution rates. Bondietti et al. (1993) found a similar inhibitory effect of citrate on the EDTA-promoted dissolution of lepidocrocite at pH 3. They interpreted the inhibitory effect as the result of adsorption competition between citrate and EDTA. Although citrate is an iron chelating ligand that is capable of promoting iron (hydr)oxide dissolution (Zhang et al., 1985), it is less efficient in promoting dissolution compared to EDTA (Nowack and Sigg, 1997). The effect of adsorption competition between EDTA and citrate on ligand-controlled dissolution rates was successfully modeled with the rate law of ligand-controlled dissolution Eq. (1) (Bondietti et al., 1993).

3.3. Dissolution of goethite in the presence of DFO-B and oxalate under non-steady-state conditions

Fig. 3 shows iron concentrations as a function of time in a batch goethite dissolution experiment with consecutive additions of the siderophore DFO-B. For comparison, goethite dissolution in the presence of constant total DFO-B concentrations (lower solid line) and DFO-B and oxalate concentrations (upper solid line) were calculated from rates that have been reported above. The filled circles represent dissolved iron concentrations in a goethite suspension that initially did not contain any organic ligands. Repeated additions of small volumes of DFO-B stock solution triggered slow dissolution of goethite (arrows indicate times of DFO-B additions and resulting concentration increases are indicated above the arrows in Fig. 3). No iron dissolution was observed before the first siderophore addition. After the first addition, net dissolution rates were approximately equal to the rates observed in dissolution experiments in the presence of constant siderophore concentrations (lower solid line) even though the total DFO-B concentrations were higher in the latter experiments. This

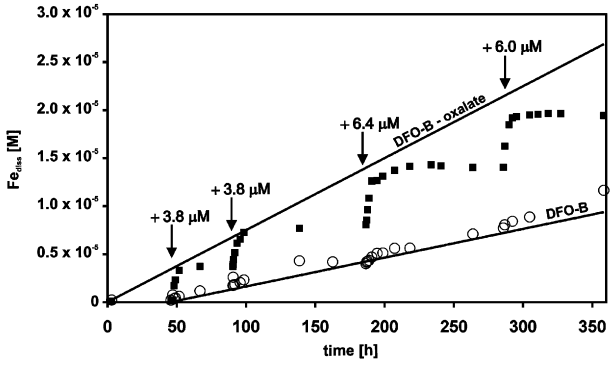

Fig. 3. Effect of pulse additions of DFO-B on goethite dissolution in a suspension containing no oxalate (circles) and a suspension with a total oxalate concentration of 5.0×10^{-5} M (squares). The times of DFO-B additions are indicated by arrows and added DFO-B concentrations are indicated above the arrows. The solid lines show calculated goethite dissolution in the presence of constant total concentrations of DFO-B (4.0×10^{-5} M, lower line) and of DFO-B (5.0×10^{-5} M) and oxalate (5.0×10^{-5} M) (upper line). 2.5 g L^{-1} goethite solid concentration, I = 0.01 M ($NaClO_4$), pH 6.

insensitivity of the DFO-B promoted dissolution rates to the DFO-B concentrations is a consequence of the shape of the DFO-B adsorption isotherm, where maximum surface capacities are approached in the low micromolar concentration range (Kraemer et al., 1999).

The presence of a constant oxalate concentration of 5.0×10^{-5} M in an otherwise identical experiment had an important effect on the response of the system to the non-steady-state conditions induced by repeated siderophore additions (Fig. 3, square symbols). Before the first DFO-B addition, when oxalate was the only organic ligand present in the goethite suspension, measured dissolved iron concentrations were within the 2-fold standard deviation of the detection limit and were therefore considered as zero. After the first addition of DFO-B, a fast dissolution of iron was observed until dissolved iron concentrations were equal to the added DFO-B concentrations and remained approximately constant. The constant iron concentration corresponds to the goethite solubility under the experimental conditions as predicted by equilibrium calculations using the constants listed in Table 1. Hence, the concentrations of iron released by the fast dissolution reaction in this experiment may even have been higher if higher concentrations of DFO-B would have been added. Reproducible fast dissolution reactions were triggered by each consecutive siderophore addition. The concentrations of iron released in the fast dissolution reactions matched the concentration of iron released in dissolution experiments at constant DFO-B and oxalate concentrations (upper solid line). To fully model the approach of iron concentrations to solubility equilibrium seen the experiment (Fig. 3) it would be necessary to apply a rate law that explicitly takes into account the effect of the solution saturation state on net dissolution rates such as Eq. (1).

In summary, non-steady-state conditions induced by the additions of DFO-B caused a fast mobilization of iron only when oxalate was present. Before the addition of the siderophore, no dissolution of iron was observed. Therefore, we assume that the presence of oxalate led to a labilization of iron surface sites and that the rapid detachment of labile iron was triggered by the step-wise increase of the DFO-B concentration.

3.4. Isotopic exchange

As discussed above, we assume that the fast dissolution reaction as a response to non-steady-state conditions implies the presence of a kinetically labile iron pool that increases over time in the presence of oxalate. However, one may argue that the addition of the siderophore is not just triggering the release of labile iron into the solution, but that it is actively involved in the labilization of the iron at the mineral surface. To investigate the existence of labile iron before the addition of the siderophore, an isotopic exchange experiment was carried out. To avoid a possible disturbance of the system by the addition of the ^{59}Fe, a total oxalate concentration of 8.0×10^{-3} M was added resulting in an elevated constant concentration of dissolved iron of 3.4×10^{-5} M after a reaction time of 1490 h. Fig. 4 shows the results of the isotopic exchange experiment. The addition of 7.28×10^{-9} M of ^{59}Fe-labeled iron to the goethite suspension did not have a significant effect on the measured concentration of dissolved iron of 3.4×10^{-5} M. The activity in solution (diamonds) decreased immediately (within 30 s) until a new isotopic equilibrium was reached. Twenty-nine hour after the addition of ^{59}Fe, 1.0×10^{-4} M DFO-B was added. This triggered a fast non-steady-state dissolution reaction and a concomitant increase of the ^{59}Fe activity in solution. Considering that only trace amounts of ^{59}Fe with a low activity of 328 Bq mL^{-1} was added to goethite suspension, we expect no significant radiation damage to the goethite. Also, Brantley et al. (2004) observed no iron isotope fractionation by DFO-B-promoted dissolution of

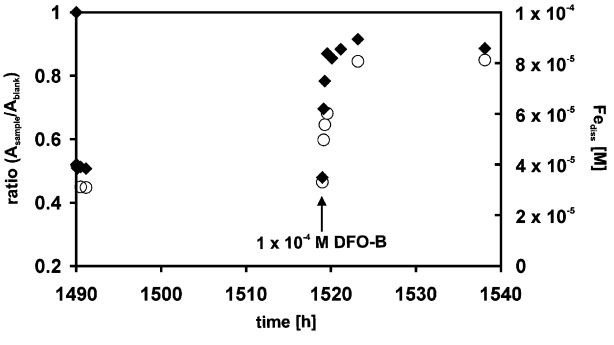

Fig. 4. Isotopic exchange of labile surface iron with ^{59}Fe. 7.28×10^{-9} M ^{59}Fe-labeled iron was added at $t = 1490$ h. 1.0×10^{-4} M DFO-B was added at $t = 1519$ h. The ratios of the activity of the filtered suspension and the activity of a blank containing the same total ^{59}Fe concentration (diamonds) are plotted as a function of time (left axis: A_{sample}/A_{blank}). Total dissolved iron concentrations are represented by open circles (right axis). Solid concentration: 2.5 g L^{-1}, $[oxalate]_{total} = 8.0 \times 10^{-3}$ M, $I = 0.01$ M ($NaClO_4$), pH = 6.0 ± 0.05.

goethite, so that an effect of ^{59}Fe on dissolution rates is not expected.

Assuming that the ^{59}Fe-labeled iron partitioned into an exchangeable iron pool at the goethite surface and that the ratio of labeled and non-labeled Fe was the same in solution and in the surface pool at equilibrium, the concentration of the labile iron pool at the goethite surface was calculated applying mass balance. From the isotopic exchange experiment, an exchangeable pool of $3.94 \times 10^{-5} \pm 3.5 \times 10^{-6}$ M, Fe was calculated (corresponding to a surface concentration of the exchangeable pool of $4.15 \times 10^{-7} \pm 3.7 \times 10^{-8}$ mol m^{-2}) which compared well with the fast non-steady-state dissolution of $4.4 \times 10^{-5} \pm 1.4 \times 10^{-6}$ M iron after addition of 1.0×10^{-4} M DFO-B.

Koretsky et al. (1998) calculated densities of iron atoms on goethite surfaces between 4.4 nm^{-1} (010) and 7.2 nm^{-1} (100) within 1.4 Å depth. Using these calculated iron site densities, a 'monolayer' of iron on goethite (i.e. iron surface site densities within 1.4 Å of perfect (010) and (100) surfaces) between 7.3×10^{-6} mol m^{-2} and 1.2×10^{-5} mol m^{-2} can be estimated. The surface concentration of the exchangeable pool of 4.15×10^{-7} mol m^{-2} thus corresponds to only 3–6% of a monolayer of reactive surface iron as defined above.

In this experiment we observed a rapid exchange of ^{59}Fe in solution with iron of natural isotopic composition in the labile pool. From the rates and extent of isotopic exchange, we were able to independently estimate the kinetic properties and surface concentration of the labile pool. In conclusion, the isotopic exchange experiment confirmed the creation of a labile iron pool in the presence of oxalate independently of non-steady-state conditions induced by siderophores. It is interesting to note, that approximately 10% of the ^{59}Fe which exchanged into the labile pool was not re-dissolved in the fast non-steady-state dissolution reaction. This observation implies that some of the ^{59}Fe in the labile pool exchanged with more stable iron pools at the mineral surface.

3.5. Influence of the oxalate concentration on the dissolution under non-steady-state conditions

As discussed above, the presence of oxalate is a prerequisite for the formation of a labile pool at the mineral surface. A series of experiments was designed to investigate if a linear relationship between adsorbed ligand concentrations and rates of labile pool formation exists. The existence of such a relationship would indicate that the rate law of oxalate-promoted dissolution can be applied to model the rates of formation of a labile iron pool in the presence of oxalate. Five non-steady-state batch dissolution experiments in the presence of different oxalate concentrations (0, 2.5×10^{-5}, 5.0×10^{-5}, 7.5×10^{-5}, and 1.0×10^{-4} M oxalate) were conducted (Fig. 5a). To induce non-steady-state conditions,

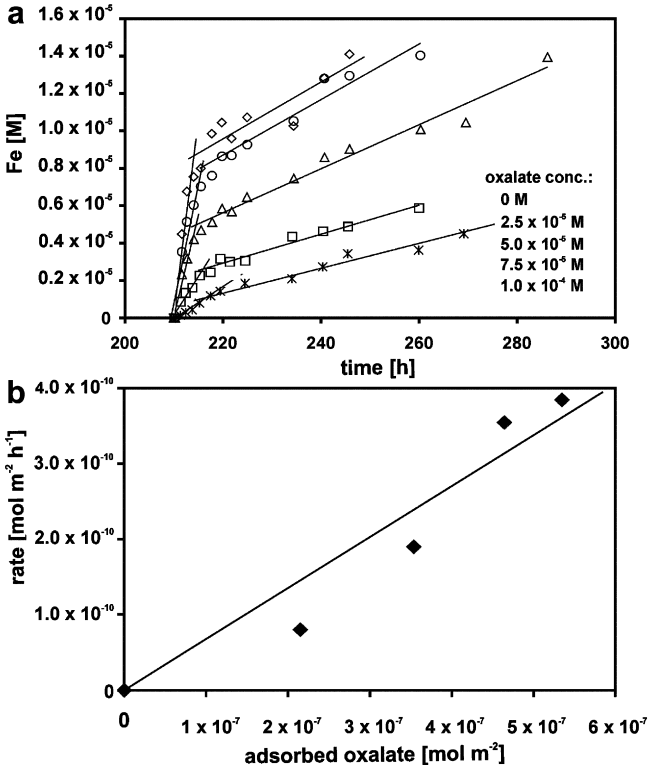

Fig. 5. (a) Fast dissolution under non-steady-state conditions in the presence of different oxalate concentrations. The data represent the results of five dissolution experiments with oxalate concentrations of 0, 2.5×10^{-5}, 5.0×10^{-5}, 7.5×10^{-5}, and 1.0×10^{-4} M, respectively. 4.0×10^{-5} M DFO-B was added at $t = 210$ h in each experiment. Solid lines represent results of linear least squares calculations for the fast dissolution reactions and subsequent slow dissolution reactions. Solid concentration of goethite: 2.5 g L^{-1}, ionic strength: 0.01 M ($NaClO_4$), pH 6. (b) Correlation between rates of labile pool formation (see Table 4) and adsorbed oxalate concentrations. Adsorbed oxalate concentrations are taken from Fig. 1.

4.0×10^{-5} M DFO-B was added after 210 h in all batch experiments. In the presence of oxalate, DFO-B additions triggered fast non-steady-state dissolution of iron. The fast dissolution reaction was followed by slow dissolution. Solutions were still far from equilibrium at the end of each experiment. Even at the highest iron concentrations (14 μM) observed in these experiments the calculated ΔG is −27 kJ/mole and no significant effect of solution saturation state on net dissolution rates is predicted according to Eqs. (1) and (2). The concentration of labile iron increased with increasing oxalate concentrations. Dissolution rates of the fast dissolution reaction were calculated based on the experimental data of the first four hours after the siderophore additions (Table 4). The dissolution rate corresponds to the slope calculated by linear least squares analysis. The rate is reported with calculated 95% confidence limits on the slope from the regression analysis. Dissolution rates of the subsequent slow dissolution reaction were calculated in the same way, using experimental data that were collected after four hours past the siderophore additions. The calculated regression lines for fast and slow dissolution are plotted in Fig. 5a as solid lines.

The highest rate of the fast dissolution reaction ($2.2 \times 10^{-8} \pm 2.4 \times 10^{-8}$ mol h^{-1} m^{-2}, see Table 4) was observed in the experiment with the highest oxalate concentration of 10^{-4} M. This rate was about fife times slower than the rate of the fast dissolution reaction observed in the isotopic exchange experiment at an even higher total oxalate concentration of 8×10^{-3} M.

The iron concentrations at the intercepts of the regression lines for the fast and the subsequent slow dissolution correspond to the concentrations of the labile iron pool $[Fe]_{lab_{total}}$. In the absence of oxalate, no significant fast dissolution of iron occurred and constant low net dissolution rates were observed after addition of DFO-B. It is important to note that fast dissolution of 1.2×10^{-6} M kinetically labile iron was observed even in the absence of oxalate. This labile iron concentration corresponds approximately to iron released in fast initial dissolution reaction observed in dissolution experiments with constant ligand concentrations (1.6×10^{-6} M; see Fig. 2). As discussed above, fast initial dissolution strongly depends on synthesis and pre-treatment of the mineral and is commonly observed in iron oxide dissolution studies. Assuming that the total kinetically labile iron at the oxide surface $[Fe]_{lab_{total}}$ is the sum of labile iron present initially $[Fe]_{lab_{initial}}$ and of the labile iron that is generated in the reaction with oxalate $[Fe]_{lab_{ox}}$, the rate of labile pool formation can be calculated by Eq. (7):

$$R = \frac{\left([Fe]_{lab_{total}} - [Fe]_{lab_{initial}}\right)}{t \times A} = \frac{[Fe]_{lab_{ox}}}{t \times A} \quad (7)$$

where R is the surface area normalized rate of labile pool formation [mol h^{-1} m^{-2}], $[Fe]_{lab_{total}}$ is the concentration of kinetically labile iron released in the fast dissolution reaction [M], $[Fe]_{lab_{initial}}$ is the concentration of kinetically labile iron released in the fast dissolution reaction in the absence of oxalate [M], t is the time before siderophore addition (i.e. $t = 210$ h), and A is the goethite surface area in suspension [m^2 L^{-1}]. The rates of labile pool formation as a function of adsorbed oxalate concentrations are plotted in Fig. 5b. Adsorbed oxalate concentrations were calculated using a Freundlich isotherm model (Fig. 1). Under the experimental conditions, the adsorbed oxalate concentrations always significantly exceeded the surface concentrations of kinetically labile iron. Interestingly, the release of labile iron in the presence of 5.0×10^{-5} M DFO-B after 210 h reaction time was lower than the iron concentrations released in the experiment where multiple DFO-B additions have been added (Fig. 3). The additional iron released may be due to a siderophore promoted surface controlled dissolution mechanism which contributes to dissolution after the first addition of DFO-B in Fig. 3.

The linear relationship between adsorbed oxalate concentration and the rates of labile pool formation (Fig. 5b) indicates that the labilization reaction follows the same rate law as ligand-controlled dissolution. The slope of the plot corresponds to the rate coefficient of oxalate-promoted labile pool formation and was calculated as 0.0007 h^{-1}. This compares well with the dissolution rate coefficient of oxalate-promoted dissolution of 0.001 h^{-1} at pH 5 reported by Cheah et al. (2003) and with the ligand-controlled dissolution rate coefficient k_{ox} of 0.0013 h^{-1} calculated with Eq. (5). Considering the correspondence of the rate law and the rate constants we hypothesize that the oxalate-promoted labilization of iron at the mineral surface and the oxalate-promoted dissolution mechanisms share the same rate-determining reaction step.

3.6. Formation of kinetically labile iron at iron oxide surfaces in the presence of low molecular weight organic acids other than oxalate

We demonstrated that oxalate promotes the formation of kinetically labile iron at the goethite surface and that the process of labilization does not occur in the absence of an organic ligand. To test if this process is resulting from

Table 4
Rates of DFO-B-controlled dissolution of goethite at pH 6 in the presence of different oxalate concentrations

Oxalate [M]	R_{fast} [mol m^{-2} h^{-1}]	R_{slow} [mol m^{-2} h^{-1}]	$[Fe]_{lab_{total}}$ [M]	$[Fe]_{lab_{ox}}$ [M]	$R_{Fe_{lab}}$ [mol m^{-2} h^{-1}]
0	$0.2 \times 10^{-8} \pm 0.08 \times 10^{-8}$	$0.7 \times 10^{-9} \pm 0.20 \times 10^{-9}$	1.2×10^{-6}	0	0
2.5×10^{-5}	$0.4 \times 10^{-8} \pm 0.16 \times 10^{-8}$	$0.7 \times 10^{-9} \pm 0.09 \times 10^{-9}$	2.8×10^{-6}	1.6×10^{-6}	0.8×10^{-10}
5.0×10^{-5}	$1.1 \times 10^{-8} \pm 0.8 \times 10^{-8}$	$1.2 \times 10^{-9} \pm 0.2 \times 10^{-9}$	4.9×10^{-6}	3.8×10^{-6}	1.9×10^{-10}
7.5×10^{-5}	$1.3 \times 10^{-8} \pm 0.9 \times 10^{-8}$	$2.1 \times 10^{-9} \pm 0.2 \times 10^{-9}$	8.3×10^{-6}	7.1×10^{-6}	3.6×10^{-10}
1.0×10^{-4}	$2.2 \times 10^{-8} \pm 2.4 \times 10^{-8}$	$1.2 \times 10^{-9} \pm 0.3 \times 10^{-9}$	8.8×10^{-6}	7.6×10^{-6}	3.9×10^{-10}

Net dissolution rates and 95% confidence limits were calculated by linear regression and normalization to the goethite surface area. The rate of labile pool formation is $R_{Fe_{lab}} = \frac{[Fe]_{lab_{ox}}}{t \times A}$ where $[Fe]_{lab_{ox}}$ is the concentration of labile iron minus the concentration of labile iron present before reaction with oxalate, t is the reaction time before DFO-B addition and A represents the surface area.

a unique property of oxalate, we substituted oxalate with citrate or malonate in non-steady-state dissolution experiments (Fig. 6). In each batch, non-steady-state was induced by the addition of 4.0×10^{-5} M DFO-B. For all three organic acids (oxalate, malonate, and citrate) a fast dissolution of iron was observed after the addition of the siderophore. In the presence of oxalate, iron was most effectively dissolved under non-steady-state conditions. In all three experiments, the fast non steady-state dissolution reaction was followed by a slower dissolution reaction. Although citrate exhibited an inhibitory effect on goethite dissolution in the presence of constant DFO-B concentrations (Fig. 2), a fast mobilization of iron was also observed under non-steady-state conditions but the labile iron pool was small compared to the experiments involving oxalate and malonate.

In summary, these experiments indicate that the labilization of iron at the mineral surface is not only promoted by oxalate but also by other low molecular weight organic acids such as citrate and malonate.

3.7. Effect of organic ligands other than DFO-B on the dissolution of kinetically labile iron from iron oxide surfaces

To investigate if fast dissolution reactions are also triggered by ligands other than DFO-B, we substituted DFO-B with the fungal siderophore ferrichrome, the phytosiderophore DMA and the low molecular weight organic acid citrate (Fig. 7). To create kinetically labile iron at the goethite surface, the low molecular weight organic acid oxalate (1.0×10^{-4} M) was chosen in all experiments. To induce non-steady-state conditions, 4.0×10^{-5} M DFO-B, 4.0×10^{-5} M ferrichrome, 3.0×10^{-3} M DMA or 3.0×10^{-3} M citrate were spiked to the respective oxalate–goethite suspensions. The concentrations of the ligands were high enough to allow the dissolution of the labile pool without reaching a new thermodynamic equilibrium that would preclude further dissolution during the experiment. A fast non-steady-state dissolution was triggered by the addition of all ligands investigated here, followed by slow net dissolution rates. The rates of the fast non-steady-state dissolution reactions triggered by DFO-B, ferrichrome, Citrate, and DMA were 3.3×10^{-8}, 12.0×10^{-8}, 3.8×10^{-8}, and 4.7×10^{-8} mol m^{-2} h^{-1}, respectively. Variations in the concentrations of labile iron released in the four experiments are in part due to variations in reaction time (compare Fig. 7a and c). However, the concentration of iron released in the fast reaction depended also on the type of siderophore added (compare Fig. 7a and b). The larger effect of ferrichrome compared to DFO-B on fast initial dissolution seems to correlate with higher dissolution rates in the presence of ferrichrome after the release of labile iron from the surface. This seems to indicate that ferrichrome is more efficient in promoting dissolution in a surface-controlled mechanism compared to DFO-B, and that it attacks and dissolves surface sites in a fast reaction that are not participating in the fast dissolution reaction in the presence of DFO-B. However, additional work is required to address the specific differences in the effect of siderophores with different structures.

Nevertheless, the observation that all added siderophores and citrate triggered the release of labile iron indicates that the fast mobilization of iron is not exclusive for the siderophore DFO-B. Thus, fast non-steady-state dissolution of iron can be induced by any ligand that is added with a concentration that sufficiently shifts the solution saturation state to allow a fast non-steady-state dissolution.

3.8. Dissolution mechanism

Samson and Eggleston (2002) observed fast goethite dissolution reactions in response to rapid pH changes (e.g. pH 4.5 was dropped rapidly to pH 1 triggering a fast dissolution reaction). They suggested that the increasing hydroxylation of the goethite surface with increasing pH accelerated ligand exchange reactions at surface metal centers which led to a change in the surface site distribution within minutes. They assumed that the newly formed surface species were precursors of the fast dissolution reaction that was assisted by protonation and depolymerization after the pH drop (Samson and Eggleston, 1998, 2000, 2002). Interestingly, we did not see fast dissolution reactions as a response to

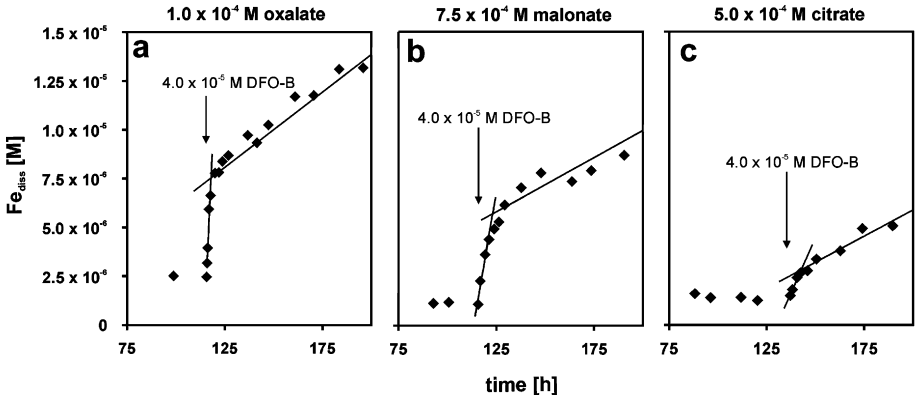

Fig. 6. Fast non-steady-state dissolution in the presence of three different labilizing ligands: 1.0×10^{-4} M oxalate (a), 7.5×10^{-4} M malonate (b), and 5.0×10^{-4} M citrate (c). Non-steady-state conditions were induced by additions of 4.0×10^{-5} M DFO-B. Solid concentration of goethite 2.5 g L^{-1}, $I = 0.01$ M ($NaClO_4$), pH 6.

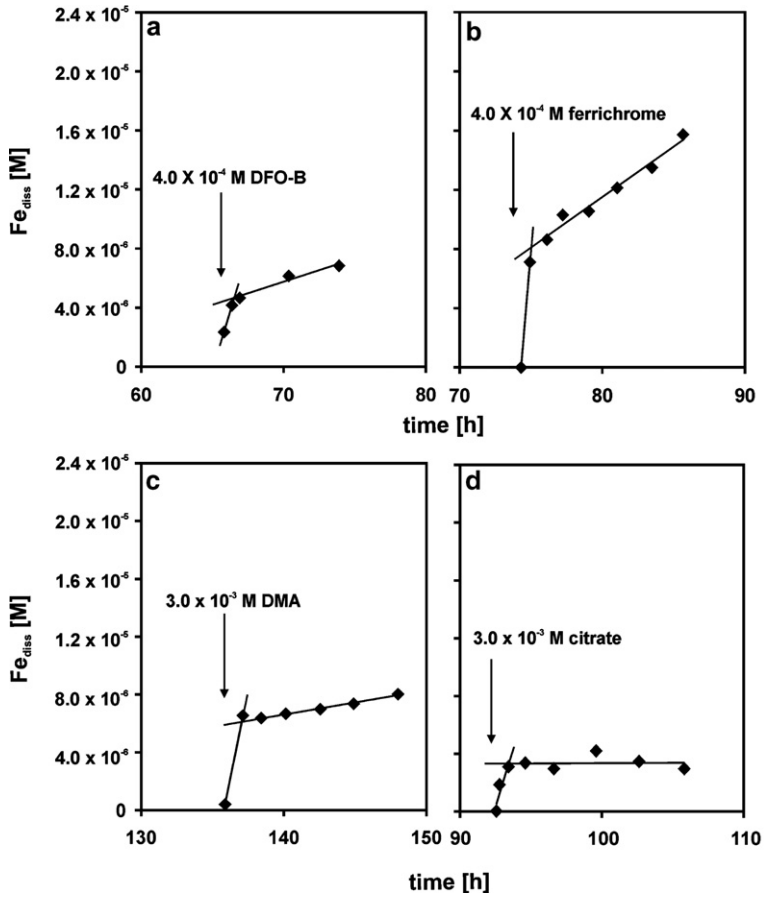

Fig. 7. Fast non-steady-state dissolution in the presence of oxalate triggered by additions of four different ligands: 4.0×10^{-5} M DFO-B (a), 4.0×10^{-5} M ferrichrome (b), 3.0×10^{-3} M DMA (c), and 3.0×10^{-3} M citrate (d). $[\text{oxalate}]_{\text{total}} = 1.0 \times 10^{-4}$ M. Solid concentration of goethite: 2.5 g L^{-1}, $I = 0.01$ M ($NaClO_4$), pH 6.

DFO-B additions to goethite suspensions in the absence of an organic ligand (see Fig. 3). This seems to indicate that the detachment of surface sites that are created by the process that has been described by Samson and Eggleston (2002) is not triggered by changes of the solution saturation state or by a DFO-B-promoted surface-controlled dissolution mechanism but only by a proton-promoted mechanism. These observations are consistent with the dissolution model proposed by Furrer and Stumm (1986) that requires that proton-promoted and ligand-promoted dissolution mechanisms are independent.

In the experiments presented here, the formation of kinetically labile iron at the mineral surface requires the presence of an organic ligand. It is difficult to infer the bonding environment of the kinetically labile iron in the absence of spectroscopic information. The formation of the kinetically labile iron pool is not consistent with the precipitation of iron oxalate salts. As discussed above, maximum soluble iron concentrations are extremely low ($<10^{-10}$ M) before addition of the siderophore due to the low solubility of goethite. Surface precipitation of iron oxalate salts would require extremely high thermodynamic stabilities of the precipitates. However, di- and trivalent metal oxalate precipitates have a high solubility relative to the low concentration of iron and oxalate during accumulation of the labile iron (Harrison and Thyne, 1992; Martell et al., 2001).

Oxalate adsorbs rapidly at iron oxide surfaces by a ligand exchange reaction that results in the formation of bidentate inner sphere surface complexes (Stumm and Sulzberger, 1992). The formation of such surface complexes increases ligand exchange rates around surface metal centers (Casey and Westrich, 1992; Casey and Ludwig, 1996). Similarly, to the model proposed by Samson and Eggleston (2002), we suggest that this process accelerates changes of the surface site distribution. Bidentate inner sphere oxalate surface complexes are thus precursors of the reaction step that results in the formation of kinetically labile surface complexes. The dissolution reaction involves the exchange of structural oxygen and hydroxyl groups by water in the inner coordination sphere of iron at the mineral surface (Casey and Ludwig, 1996). Iron in goethite is octahedrally coordinated and several bonds are exchanged during dissolution (Casey and Ludwig, 1996). It has been suggested that these multiple exchange reactions involve multiple elementary reactions and intermediates (Kraemer and Hering, 1997). This is consistent with dissolution models where dissolving ions pass through a series of surface

microtopographical sites (e.g. plane, step, kink, ledge, and adatom) before detachment from the surface (Burton et al., 1951; Maurice et al., 1995). This is particularly relevant for the interpretation of non-steady-state experiments as the concentration of intermediates can change as a function of solution saturation state: far from equilibrium their concentrations are determined by the kinetics of the dissolution process, at equilibrium their concentrations are determined by their thermodynamic stabilities. In this context we interpret the formation of the labile iron pool as an oxalate-promoted formation and accumulation of intermediates in this multiple step reaction. The fast dissolution reaction results in the depletion of these intermediates. In terms of the microtopographical interpretation of this model, the depletion of the labile iron is equivalent to the disappearance of surface sites with low lattice coordination such as ledge sites and/or adatoms. Further validation of this concept will require spectroscopic or microscopic investigations of the labile surface sites.

The rate law Eq. (1) is based on a conceptual model of the ligand-controlled dissolution involving three steps: the formation of the precursor to the dissolution reaction (i.e. the coordination of surface metal centers by a ligand via a ligand exchange reaction), the slow, rate determining detachment of the coordinated metal center (i.e. its dissolution) and a fast protonation of the mineral surface (Furrer and Stumm, 1986).

We propose a conceptual model of ligand-controlled dissolution in the presence of constant total ligand concentrations and under non-steady-state conditions (Fig. 8) that is an extension of the model by Furrer and Stumm (1986). The model conceptually recognizes a precursor of the labilization reaction (i.e. a surface iron center that is coordinated by the organic ligand) and intermediates of the dissolution reaction that are formed by depolymerization of the precursor of the labilization reaction (the labile iron surface species). The conceptual model involves the following reaction steps:

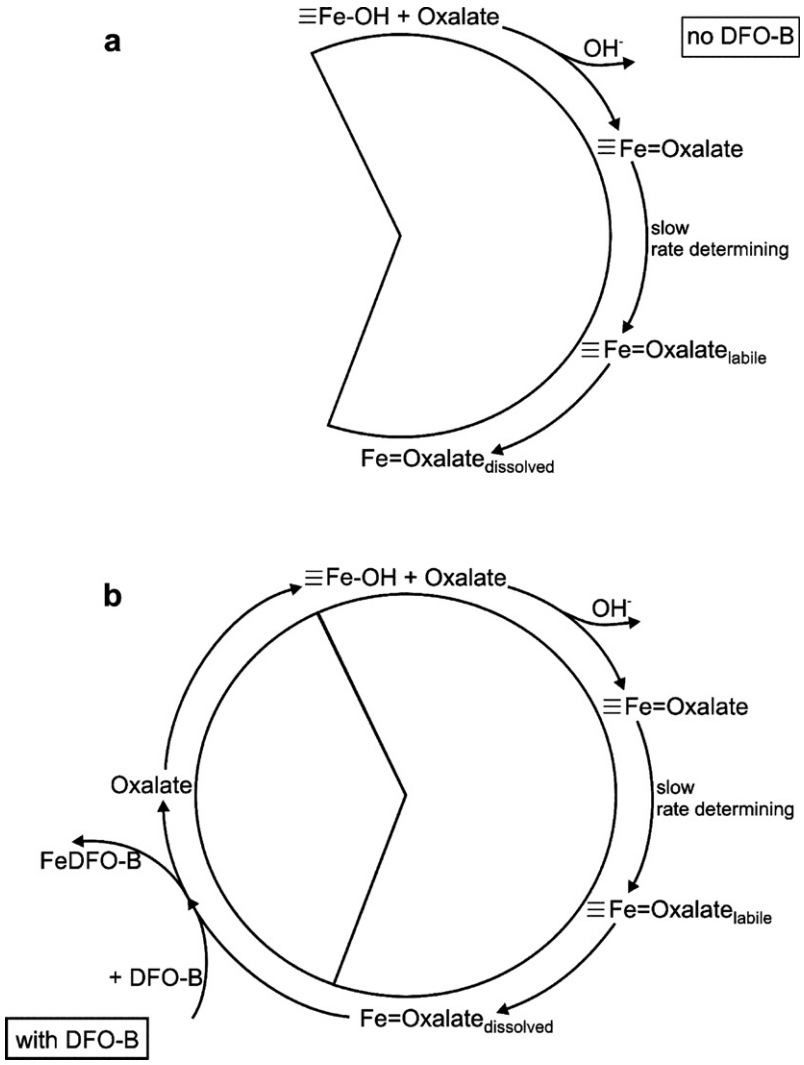

Fig. 8. Mechanism of fast iron dissolution in the presence of oxalate (a) without and (b) with DFO-B. In the absence of DFO-B, labile surface complexes are accumulating at the oxide surface with time (a). Upon addition of DFO-B, the labile surface complexes are depleted in a fast non-steady-state dissolution reaction (b).

- adsorption of an organic ligand by a ligand exchange reaction,
- the slow formation of a kinetically labile iron surface species (which is an intermediate in the dissolution reaction),
- detachment of the labile surface species,
- rapid ligand exchange reactions in solution,
- rapid re-adsorption of organic ligands/re-protonation of the surface.

At constant siderophore concentrations and under far from equilibrium conditions, the overall dissolution rate will be controlled by the slow formation of a kinetically labile iron surface species. This labile intermediate will rapidly detach from the surface so that its surface concentration is low. Hence, ligand-controlled dissolution under these conditions is consistent with the accepted conceptual model and corresponding rate law of ligand-controlled dissolution (Eq. 1).

Non-steady-state experiments are characterized by a rapid shift in solution saturation state upon addition of the siderophore. As discussed above, the low solubility of goethite limits dissolution in the presence of oxalate, malonate, and citrate. As equilibrium is approached, the rate of detachment of the labile intermediates goes to zero while the formation of the labile intermediates continues until an equilibrium surface speciation is established (Fig. 8a). The addition of the siderophore strongly shifts the saturation state to negative ΔG values (<-28 kJ mol^{-1}, see Table 2). The system responds to this by a rapid detachment of kinetically labile iron until the labile iron pool is depleted (Fig. 8b). After the depletion of the labile iron pool, net dissolution rates are controlled by the slow labilization reaction and correspond to dissolution rates in the presence of constant total ligand concentrations. If a new equilibrium is approached net dissolution rates decrease once again and a new labile iron pool is established. The reproducible observation of fast non-steady-state dissolution (Fig. 3) is consistent with a cyclic accumulation and release of the kinetically labile iron pool.

The detachment of the labile iron is immediately followed by a ligand exchange reaction where the low molecular weight organic ligands (e.g. oxalate, malonate or citrate) are substituted by siderophores in the coordination sphere of dissolved iron. If the rate of the ligand exchange reaction is slow, it could limit the rate of detachment of the labile iron from the surface. However, the linear relationship between adsorbed oxalate and the detachment rate (Fig. 5b) seems to indicate a surface-control of the detachment step. Oxalate, malonate, and citrate are catalysts in this reaction scheme as they are released by the ligand exchange reaction in solution and may participate in the reaction again (Fig. 8b). In the absence of this catalyst we did not observe the labilization reaction (Fig. 3).

4. CONCLUSIONS

We observed a fast goethite dissolution reaction in the presence of oxalate as a response to changes in the solution saturation state triggered by increasing DFO-B concentrations. This process is highly reproducible, because the labile pool can be repeatedly regenerated in the presence of oxalate. Therefore, this process is different from fast initial dissolution that is commonly observed in dissolution studies. We observed the formation of kinetically labile iron at the mineral surface in the presence of several labilizing organic ligands (oxalate, malate, and citrate) that are commonly found in soils and aqueous systems. Also, we showed that the rapid mobilization of the labile iron can be triggered by siderophores or other organic ligands with a high affinity for the formation of soluble iron complexes. It is a general mechanism triggered by the induction of changes in the solution saturation state by the addition of a strong iron-chelating ligand.

It is likely that this mechanism is important for mineral weathering and nutrient acquisition processes in dynamic natural systems where diurnal changes in the solution saturation state occur. An example is the iron acquisition by iron limited graminaceous plants that exude siderophores into the rhizosphere in a diurnal pattern (Römheld, 1991). The pulse-like exudation of siderophores minimizes microbial degradation and maximizes the local concentration of the siderophore during periods of maximum exudation. Fast non-steady-state dissolution reactions can contribute to efficient iron acquisition during the short exudation period.

ACKNOWLEDGMENTS

We are grateful to Prof. Volker Römheld and Dr. Günther Neumann (Universität Hohenheim) for their help in setting up the phytosiderophore purification and analysis methods. We also thank Kurt Barmettler for technical support and Paul Borer for assistance in the ^{14}C and UV measurements. Detailed comments and revisions by Eric Oelkers, Sherri Samson, and two anonymous reviewers are greatly appreciated. This work was supported by ETH Zürich, Grant # 16./00-3.

APPENDIX A. SUPPLEMENTARY DATA

Supplementary data associated with this article can be found, in the online version, at doi:10.1016/j.gca.2006.12.022.

REFERENCES

Aagaard P. and Helgeson H. C. (1982) Thermodynamic and kinetic constraints on reaction-rates among minerals and aqueous-solutions. 1. Theoretical considerations. *American Journal of Science* **282**, 237–285.

Albrecht-Gary A.-M. and Crumbliss A. L. (1998) Coordination chemistry of siderophores: thermodynamics and kinetics of iron chelation and release. In *Metal Ions in Biological Systems*, vol. 35 (eds. A. Sigel and H. Sigel). Marcel Dekker, New York, pp. 239–327.

Allison M. J., Daniel S. L. and Cornick N. A. (1995) Oxalate-degrading bacteria. In *Calcium Oxalate in Biological Systems* (ed. S. R. Khan). CRC Press, FL, pp. 131–168.

Bondietti G., Sinninger J. and Stumm W. (1993) The reactivity of Fe(III)(hydr)oxides: effects of ligands in inhibiting the dissolution. *Colloid. Surface A* **79**, 157–167.

Borer P. M., Sulzberger B., Reichard P. U. and Kraemer S. M. (2005) Effect of siderophores on the light-induced dissolution of colloidal iron (III)(hydr)oxides. *Mar. Chem.* **73**, 179–193.

Brantley S. L., Liermann L. J., Guynn R. L., Anbar A., Icopini G. A. and Barling J. (2004) Fe isotopic fractionation during mineral dissolution with and without bacteria. *Geochim. Cosmochim. Acta* **68**, 3189–3204.

Burton W. K., Cabrera N. and Frank F. C. (1951) The growth of crystals and the equilibrium structure of their surfaces. *Physiol. Trans. R. Soc. Lond. A Math Phys. Sci.* **243**, 299–358.

Casey W. H. and Ludwig C. (1996) The mechanism of dissolution of oxide minerals. *Nature* **381**, 506–509.

Casey W. H. and Westrich H. R. (1992) Control of dissolution rates of orthosilicate minerals by divalent metal–oxygen bonds. *Nature* **355**, 157–159.

Cervini-Silva J. and Sposito G. (2002) Steady-state dissolution kinetics of aluminum–goethite in the presence of desferrioxamine-B and oxalate ligands. *Environ. Sci. Technol.* **36**, 337–342.

Cheah S. F., Kraemer S. M., Cervini-Silva J. and Sposito G. (2003) Steady-state dissolution kinetics of goethite in the presence of desferrioxamine B and oxalate ligands: implications for the microbial acquisition of iron. *Chem. Geol.* **198**, 63–75.

Cornell R. M. and Schindler P. W. (1980) Infrared study of the adsorption of hydroxycarboxylic acids on α-FeOOH and amorphous Fe(III)hydroxide. *Colloid Polym. Sci.* **258**, 1171–1175.

Dakora F. D. and Phillips D. A. (2002) Root exudates as mediator of mineral acquisition in low-nutrient environments. *Plant Soil* **245**, 35–47.

Fan T. W. M., Lane A. N., Pedler J., Crowley D. and Higashi R. M. (1997) Comprehensive analysis of organic ligands in whole root exudates using nuclear magnetic resonance and gas chromatography mass spectrometry. *Anal. Biochem.* **251**, 57–68.

Filius J. D., Hiemstra T. and Van Riemsdijk W. H. (1997) Adsorption of small weak organic acids on goethite: modeling of mechanisms. *J. Colloid Interf. Sci.* **195**, 368–380.

Fox T. R. and Comerford N. B. (1990) Low-molecular-weight organic-acids in selected forest soils of the southeastern USA. *Soil Sci. Soc. Am. J.* **54**, 1139–1144.

Furrer G. and Stumm W. (1986) The coordination chemistry of weathering. 1. Dissolution kinetics of Δ-Al_2O_3 and BeO. *Geochim. Cosmochim. Acta* **50**, 1847–1860.

Gadd G. M. (2000) Heterotrophic solubilization of metal-bearing minerals by fungi. In *Environmental Mineralogy* (eds. J. D. Cotter-Howells, L. S. Campbell, E. Valsami-Jones and M. Batchelder). The Mineralogical Society, London. pp. 57–75.

Gollany H. T., Schumacher T. E., Rue R. R. and Liu S.-Y. (1993) A carbon dioxide microelectrode for in situ pCO_2 measurement. *Microchem. J.* **48**, 42–49.

Harrison W. J. and Thyne G. D. (1992) Predictions of diagenetic reactions in the presence of organic acids. *Geochim. Cosmochim. Acta* **56**, 565–586.

Hersman L., Lloyd T. and Sposito G. (1995) Siderophore-promoted dissolution of hematite. *Geochim. Cosmochim. Acta* **59**, 3327–3330.

Holmen B. A. and Casey W. H. (1996) Hydroxamate ligands, surface chemistry, and the mechanism of ligand-promoted dissolution of goethite α-FeOOH(s). *Geochim. Cosmochim. Acta* **60**, 4403–4416.

Kalinowski B. E., Liermann L. J., Givens S. and Brantley S. L. (2000) Rates of bacteria-promoted solubilization of Fe from minerals: a review of problems and approaches. *Chem. Geol.* **169**, 357–370.

Koretsky C. M., Sverjensky D. A. and Sahai N. (1998) A model of surface site types on oxide and silicate minerals based on crystal chemistry: implications for site types and densities, multi-site adsorption, surface infrared spectroscopy, and dissolution kinetics. *Am. J. Sci.* **298**, 349–438.

Kraemer S. M. and Hering J. G. (1997) Influence of solution saturation state on the kinetics of ligand-controlled dissolution of oxide phases. *Geochim. Cosmochim. Acta* **61**, 2855–2866.

Kraemer S. M., Chiu V. Q. and Hering J. G. (1998) Influence of pH and competitive adsorption on the kinetics of ligand-promoted dissolution of aluminum oxide. *Env. Sci. Technol.* **32**, 2876–2882.

Kraemer S. M., Cheah S. F., Zapf R., Xu J., Raymond K. N. and Sposito G. (1999) Effect of hydroxamate siderophores on Fe release and Pb(II) adsorption by goethite. *Geochim. Cosmochim. Acta* **63**, 3003–3008.

Kraemer S. M. (2004) Iron oxide dissolution and solubility in the presence of siderophores. *Aquat. Sci.* **66**, 3–18.

Lasaga, A. C. (1981). Transition state theory. In *Kinetics of Geochemical Processes. Reviews in Mineralogy*. vol. **8**. pp. 135–169.

Marschner H. (1995) *Mineral Nutrition of Higher Plants*. Academic Press.

Martell A. E., Smith R. M. and Motekaitis R. J. (2001) *NIST Critically Selected Stability Constants of Metal Complexes*. NIST Standard Reference Database 46, Version 6.0. NIST, Gaithersburg.

Mast M. A. and Drever J. I. (1987) The effect of oxalate on the dissolution rates of oligoclase and tremolite. *Geochim. Cosmochim. Acta* **51**, 2559–2568.

Maurice P. A., Hochella M. F., Parks G. A., Sposito G. and Schwertmann U. (1995) Evolution of hematite surface microtopography upon dissolution by simple organic acids. *Clays Clay Miner.* **43**, 29–38.

Murakami T., Ise K., Hayakawa M., Kamei S. and Takagi S. (1989) Stabilities of metal complexes of mugineic acids and their specific affinities for iron(III). *Chem. Lett.*, 2137–2140.

Neilands J. B. (1974) Iron and its role in microbial physiology. In *Microbial Iron Metabolism* (ed. J.B. Neilands). pp. 3–34. Academic Press, New York.

Neumann G., Haake C. and Römheld V. (1999) Improved HPLC method for determination of phytosiderophores in root washings and tissue extracts. *J. Plant Nutr.* **22**, 1389–1402.

Nowack B. and Sigg L. (1997) Dissolution of Fe(III)(hydr)oxides by metal–EDTA complexes. *Geochim. Cosmochim. Acta* **61**, 951–963.

Parker V. B. and Khodakovskii I. L. (1995) Thermodynamic properties of the aqueous ions (2^+ and 3^+) of iron and the key compounds of iron. *J. Physic. Chem. Ref. Data* **24**, 1699–1745.

Pokrovsky O. S. and Schott J. (2004) Experimental study of brucite dissolution and precipitation in aqueous solutions: surface speciation and chemical affinity control. *Geochim. Cosmochim. Acta* **68**, 31–45.

Reichard P. U. (2005) *Effects of Microbial and Plant Siderophore Ligands on the Dissolution of Iron Oxides*. Ph.D. Thesis. Swiss Federal Institute of Technology, Zurich.

Römheld V. (1991) The role of phytosiderophores in acquisition of iron and other micronutrients in graminaceous species: an ecological approach. *Plant Soil* **130**, 127–134.

Römheld V. and Marschner H. (1986) Evidence for a specific uptake system for iron phytosiderophores in roots of grasses. *Plant Physiol.* **80**, 175–180.

Samson S. D. and Eggleston C. M. (1998) Active sites and the non-steady-state dissolution of hematite. *Environ. Sci. Technol.* **32**, 2871–2875.

Samson S. D. and Eggleston C. M. (2000) The depletion and regeneration of dissolution-active sites at the mineral–water interface: II. Regeneration of active sites on α-Fe_2O_3 at pH 3 and pH 6. *Geochim. Cosmochim. Acta* **64**, 3675–3683.

Samson S. D. and Eggleston C. M. (2002) Nonsteady-state dissolution of goethite and hematite in response to pH jumps: the role of adsorbed Fe(III). In *Water–Rock Interactions, Ore Deposits, and Environmental Geochemistry: A Tribute to David A. Crerar*, vol. 7 (ed. R. Hellmann and S. A. Wood). The Geochemical Society, pp. 61–73.

Schwertmann U. and Cornell R. M. (2000) *Iron Oxides in the Laboratory: Preparation and Characterization*. Wiley-VCH, Weinheim.

Stevenson F. J. (1967) Organic acids in soil. In *Soil Biochemistry*, pp. 119–146. Marcel Dekker, New York.

Strobel B. W. (2001) Influence of vegetation on low-molecular-weight carboxylic acids in soil solution—a review. *Geoderma* **99**, 169–198.

Stumm W. and Sulzberger B. (1992) The cycling of iron in natural environments—considerations based on laboratory studies of heterogeneous redox processes. *Geochim. Cosmochim. Acta* **56**, 3233–3257.

Sugiura Y., Tanaka H., Mino Y., Ishida T., Ota N., Inoue M., Nomoto K., Yoshioka H. and Takemoto T. (1981) Structure, properties, and transport mechanism of iron(III) complex of mugineic acid, a possible phytosiderophore. *J. Am. Chem. Soc.* **103**, 6979–6982.

Takagi S., Nomoto K. and Takemoto T. (1984) Physiological aspect of mugineic acid, a possible phytosiderophore of graminaceous plants. *J. Plant Nutr.* **7**, 469–477.

Takagi S. (1993) Production of phytosiderophores. In *Iron Chelation in Plants and Soil Microorganisms* (eds. L. L. Barton and B. C. Hemming). Academic Press, San Diego, pp. 111–131.

Telford J. R. and Raymond K. N. (1996) Siderophores. In *Comprehensive Supramolecular Chemistry* (eds. J. L. Atwood, J. E. D. Davies, D. D. Macnicol and F. Vogtle). Elsevier Science Ltd., Oxford, vol. 1, pp. 245–266.

Temkin M. I. (1971) The kinetics of steady-state complex reactions. *International Chemical Engineering* **11**, 709–717.

Teng H. H., Fenter P., Cheng L. and Sturchio N. C. (2001) Resolving orthoclase dissolution processes with atomic force microscopy and X-ray reflectivity. *Geochim. Cosmochim. Acta* **65**, 3459–3474.

Unterweger M. P., Hoppes D. D., Schima F. J. and Coursey J. S. (2001) *New and Revised Half-life Measurements Results*. NIST Physical Reference Database.

Vance G. F., Stevenson F. J. and Sikora F. J. (1996) Environmental chemistry of aluminum-organic complexes. In *The Environmental Chemistry of Aluminium* (ed. G. Sposito). CRC Press, Boca Raton, pp. 169–220.

Watteau F. and Berthelin J. (1994) Microbial dissolution of iron and aluminum from soil minerals - efficiency and specificity of hydroxamate siderophores compared to aliphatic-acids. *Eur. J. Soil Biol.* **30**, 1–9.

Zhang Y., Kallay N. and Matijevic E. (1985) Interactions of metal hydrous oxides with chelating-agents. 7. Hematite-oxalic acid and hematite-citric acid systems. *Langmuir* **1**, 201–206.

Zinder B., Furrer G. and Stumm W. (1986) The coordination chemistry of weathering. 2. Dissolution of Fe(III) oxides. *Geochim. Cosmochim. Acta* **50**, 1861–1869.

Associate editor: Eric H. Oelkers